Atmospheric and
Environmental Research, Inc.

Algorithm Theoretical Basis Document (ATBD)
for the
Conical-Scanning Microwave Imager/Sounder (CMIS)
Environmental Data Records (EDRs)

Volume 8: Total Water Content EDR

Version 1.1 – 15 March 2001

Solicitation No. F04701-01-R-0500

Submitted by:
Atmospheric and Environmental Research, Inc.
131 Hartwell Avenue
Lexington, MA 02421-3126

With contributions by:
Alan Lipton, Sid-Ahmed Boukabara, Jennifer Hegarty, Jean-Luc Moncet, Ross N Hoffman

Prepared for:
Boeing Satellite Systems
919 Imperial Avenue
El Segundo, CA 90245

AER Document P757-TR-I-ATBD-TWC-20010315

This page intentionally left blank.

REVISION HISTORY

Version	Release Date	POC	Comments
1.0	1/9/01	A. E. Lipton, AER, Inc.	First Draft Version
1.1	3/15/01	A. E. Lipton, AER, Inc.	Inserted Appendix A

RELATED CMIS DOCUMENTATION

Government Documents

Title	Version	Authorship	Date
CMIS SRD for NPOESS Spacecraft and Sensors	3.0	Associate Directorate for Acquisition NPOESS IPO	2 March 2001

Boeing Satellite Systems Documents

Title		Covering
ATBD for the CMIS TDR/SDR Algorithms		
ATBD for the CMIS EDRs	Volume 1: Overview	Part 1: Integration
		Part 2: Spatial Data Processing • Footprint Matching and Interpolation • Gridding • Imagery EDR
	Volume 2: Core Physical Inversion Module	
	Volume 3: Water Vapor EDRs	Atmospheric Vertical Moisture Profile EDR Precipitable Water EDR
	Volume 4: Atmospheric Vertical Temperature Profile EDR	
	Volume 5: Precipitation Type and Rate EDR	
	Volume 6: Pressure Profile EDR	
	Volume 7: Cloud EDRs	Part 1: Cloud Ice Water Path EDR
		Part 2: Cloud Liquid Water EDR
		Part 3: Cloud Base Height EDR
	Volume 8: Total Water Content EDR	
	Volume 9: Soil Moisture EDR	
	Volume 10: Snow Cover/Depth EDR	
	Volume 11: Vegetation/Surface Type EDR	
	Volume 12: Ice EDRs	Sea Ice Age and Sea Ice Edge Motion EDR Fresh Water Ice EDR
	Volume 13: Surface Temperature EDRs	Land Surface Temperature EDR Ice Surface Temperature EDR
	Volume 14: Ocean EDR Algorithm Suite	Sea Surface Temperature EDR Sea Surface Wind Speed/Direction EDR Surface Wind Stress EDR
	Volume 15: Test and Validation	All EDRs

Bold = this document

TABLE OF CONTENTS FOR VOLUME 8

LIST OF TABLES

LIST OF FIGURES

1 Introduction

1.1 Purpose

This algorithm theoretical basis document (ATBD) provides the underlying mathematical and theoretical background for Total Water Content (TWC) EDR (Environmental Data Record) for the Conical-scanning Microwave Imager/Sounder (CMIS) developed by Atmospheric and Environmental Research, Inc. (AER) in support of the National Polar-orbiting Operational Environmental Satellite System (NPOESS).

The total liquid water (TWC) encompasses water in all its phases. Retrievals of TWC have applications in climate and weather diagnosis and prediction that rely on analyses of the content and transport of water mass in the atmosphere.

1.2 Scope

The Core Physical Inversion Module of the CMIS EDR algorithms performs a major portion of the retrieval processing for the TWC EDR. That module is described in ATBD Vol. 2, which includes discussion of some aspects of the physics of the retrieval problem. The TWC algorithm under precipitating conditions is closely linked to the Precipitation EDR algorithm, which is described in ATBD Vol. 5. The TWC EDR product is closely related to, and is consistent with, the water vapor and cloud EDRs, which are discussed in ATBD Volumes 3 and 7, respectively. Much of the physical basis and algorithm description that provides the components of the TWC EDR is discussed in those documents. This document discusses physical aspects specific to TWC retrieval, presents the portions of the algorithm not covered by those volumes, and presents performance for the TWC EDR product.

2 Overview and Background Information

2.1 Objectives of the TWC EDR retrieval

The TWC EDR algorithm has the objective of deriving TWC reports from CMIS sensor data on a global basis in all weather conditions.

2.2 Summary of EDR requirements

2.2.1 Requirements from System Requirement Document

The text below and Table 2-1are the portions CMIS System Requirements Document (SRD) section 3.2.1.1.1.1 that apply directly to the TWC algorithm.

Total water content is defined as the water vapor, cloud liquid water, and cloud ice liquid equivalent in specified segments of a vertical column of the atmosphere. For this EDR vertical cell size is the vertical height of the column segment and the vertical reporting interval specifies the locations of the column segment bottoms for which cloud liquid water must be reported. The requirements below apply under both clear and cloudy conditions.

Table 2-1: Total Water Content Requirement Table.

Para. No.		Thresholds	Objectives
C40.3.6-1	a. Horizontal Cell Size	20 km	10 km
C40.3.6-2	b. Horizontal Reporting Interval	20 km	10 km
C40.3.6-3	c. Vertical Cell Size (TBR)	3 km	1 km
C40.3.6-4	d. Vertical Reporting Interval	Vertical cell size	Vertical cell size
C40.3.6-5	e. Horizontal Coverage	Global	Global
C40.3.6-6	f. Vertical Coverage	0 - 20 km	0 - (TBD) km
C40.3.6-7	g. Measurement Range	0 - 200 kg/m² (TBR)	(TBD)
	h. Measurement Uncertainty		
C40.3.6-8	1. Point Measurement	2 kg/m^2	(TBD)
C40.3.6-9	2. Global Average	1 kg/m^2(TBR)	(TBD)
C40.3.6-10	i. Mapping Uncertainty	7 km	7 km
C40.3.6-11	j. Swath Width	1700 km (TBR)	3000 km (TBR)

2.2.2 Interpretation of SRD Requirements

The TWC EDR definition in the SRD suggests that precipitating particles are excluded, because it refers to cloud liquid and cloud ice but does not mention precipitation. However, the measurement range stated in the requirement clearly extends to heavily precipitating clouds. Therefore, we interpret the TWC requirement as covering both precipitating and non-

precipitating clouds and encompassing all water in the atmosphere, regardless whether it is suspended in cloud particles or precipitating.

2.3 Physics of Problem

The physics involved with retrieval of vapor, liquid, and ice is discussed in ATBD Volumes 3 and 7. That material is not repeated here.

There are some similarities in the responses of microwave brightness temperatures to changes in each of the TWC components: vapor, liquid, and ice. Those similarities give rise to ambiguities between each of the components when they are retrieved from microwave data. There may, in principal, be offsetting errors between the retrieved amounts of vapor, liquid, and ice, so the retrieval of TWC would have smaller errors than the combined errors of the components. The offsetting of errors is actually very small when one takes account that the radiative responses to unit changes in the *mass* of vapor, liquid, and ice are very different. Consider, for example, non-precipitating cases. To get offsetting brightness temperature changes between an increase in cloud liquid water and a decrease in water vapor, the change in water vapor mass would need to be about 44 times the change in cloud water mass (Figure 2-1).

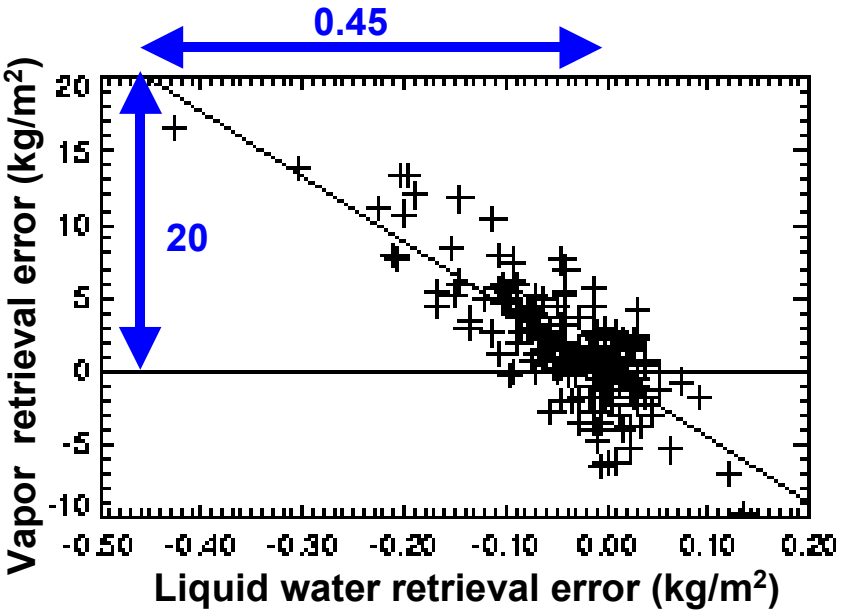

Figure 2-1: Example of retrieval ambiguity between total cloud liquid and total water vapor, in units of kg/m^2 for both variables. The retrievals were made over a high-emissivity land surface with the emissivity held to the true value.

2.4 Instrument Characteristics

The primary channels for TWC encompass all the primary channels for the Atmospheric Vertical Moisture Profile, Cloud Liquid Water, and Cloud Ice Water Path EDRs: the vertical and horizontally polarized window channels at 10, 18, 36, and 89 GHz and the water vapor channels at 23, 166 and 183 GHz. The 50-GHz channels provide temperature profile information that assists in identifying thermal effects on brightness temperatures at the other frequencies.

2.5 Requirements for cross sensor data

The TWC EDR requires real-time cross-sensor data from VIIRS for cloud top and cloud cover. The cloud cover data are used to detect clear conditions over land, eliminating the radiometric ambiguity between cloud and water vapor and improving water vapor retrieval performance. The cloud top data are used to constrain the altitude range of liquid, ice, and saturated vapor in precipitating clouds. The cloud data are also used in the quality control process (ATBD Vol. 2) to aid in identifying and flagging conditions with precipitation. The TWC EDR also requires that data from VIIRS and CrIS are used in the development and maintenance of the dynamic emissivity database that is used in the core module. For this purpose, the data need not be from the current orbit, but may be from previous recent orbits.

2.6 Requirements for External Data

The only external data required to achieve threshold performance for the TWC EDR is surface pressure, derived from combination of NWP model forecast data, and terrain heights from a high-spatial-resolution global topography database.

2.7 Summary of Derived Requirements on the EDR Algorithm

For TWC retrieval in non-precipitating conditions, the algorithm requires water vapor profile, cloud liquid water, cloud top pressure, and cloud thickness (pressure units) data from the Core Module. In precipitating conditions, the TWC algorithm produces estimates of layer liquid and ice within the Precipitation Module.

3 Algorithm Description

3.1 Historical and Background Perspective of Proposed Algorithm

TWC has not been an operational product for any previous satellite microwave sensor.

3.2 Theoretical and Mathematical Description of Algorithm

3.2.1 Non-precipitating clouds

The primary retrieval function for non-precipitating clouds is performed by the Core Physical Inversion Module. The module simultaneously retrieves the water vapor profile, total cloud liquid water, cloud top pressure, and cloud thickness. In the mode where non-precipitating ice clouds are detected, the Core Module retrieves cloud ice water path. The core module makes use of a dynamic surface emissivity database, which substantially improves performance over land surfaces. Details of the core module are in ATBD Vol. 2.

3.2.2 Precipitating clouds

3.2.2.1 Ocean areas

Liquid water path (LWP) is retrieved in the precipitation module in the course of retrieving the precipitation rate (see ATBD Vol. 5 and Vol.7, Part2). The TWC algorithm applies a neural network to the brightness temperatures and the LWP to partition the LWP among the 3-km layers over which TWC is reported. The TWC algorithm also retrieves the layer ice water path (IWP) in the same manner used to retrieve the total IWP for the CIWP EDR. In the case of TWC, the neural network is trained to do the retrieval layer-by-layer.

3.2.2.2 Land and ice areas

The layer liquid and ice are retrieved by neural network on a layer-by-layer basis. The rationale for the approach, the design of the network, and the data used to train and test it are described in ATBD Vol. 5: Precipitation.

3.2.2.3 Vapor

There is no significant skill in directly retrieving water vapor from passive microwave data in the presence of precipitation. Our algorithm maintains consistency with the moisture profile EDR by using water vapor retrieved by the Core Module in non-precipitating areas and interpolated into the precipitation areas. The interpolation procedure is described in the section of ATBD Vol. 1, Part 2 that covers gridding. The temperature profile is also interpolated and is used to compute the saturation humidity. Below cloud top, specified from VIIRS data, the interpolated water vapor is replaced by the saturated vapor profile.

3.2.3 Vertical registration

A second component of the algorithm (vertical re-mapping) takes a set of slant-path TWC profiles and performs an interpolation process to register the profile data into alignment with the local vertical. The vertical registration process is illustrated in Figure 3-1. The details of the interpolation algorithm are given in the Overview ATBD; Part 2: Footprint Matching and Interpolation. The profile retrieval step is performed separately and before the vertical registration step in order to maximize consistency between EDR algorithms.

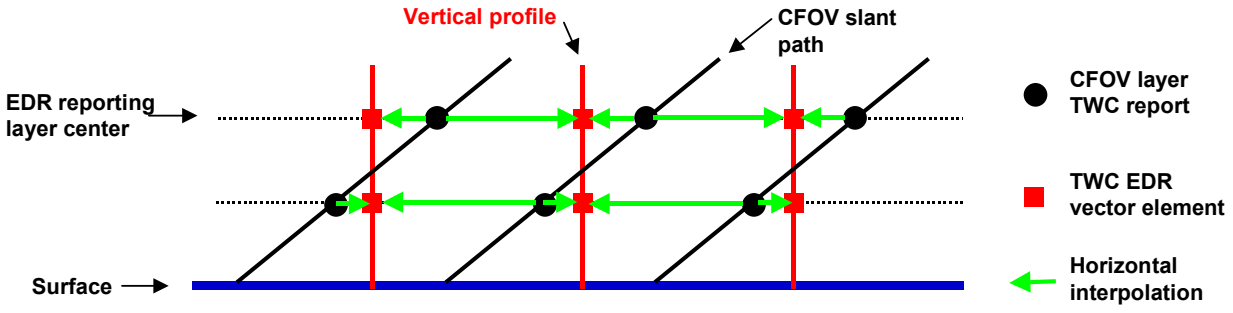

Figure 3-1: Illustration of the process of vertical registration of the TWC profile, for a cross-sectional view through a portion of a scan.

3.3 Algorithm Processing Flow

3.3.1 Processing Flow for the TWC algorithm

The primary processing flow for the TWC algorithm is illustrated in Figure 3-2. The registration to the local vertical is illustrated in Figure 3-3.

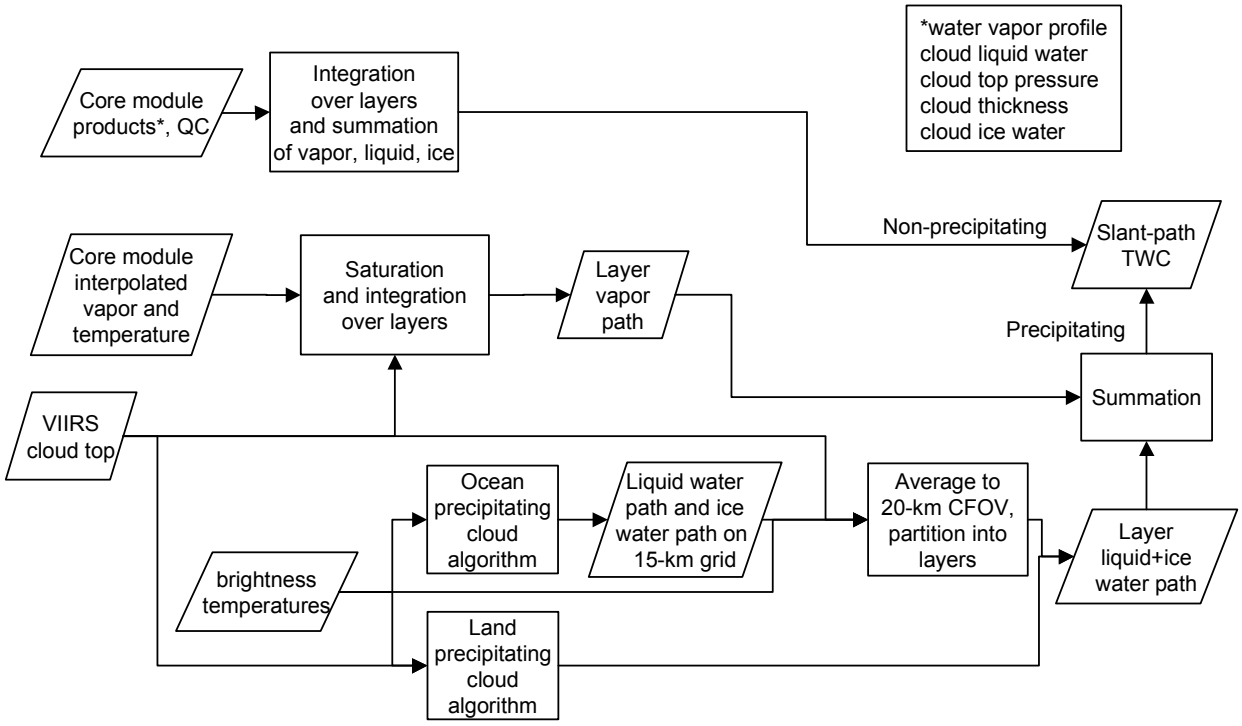

Figure 3-2: Processing flow diagram for the TWC algorithm

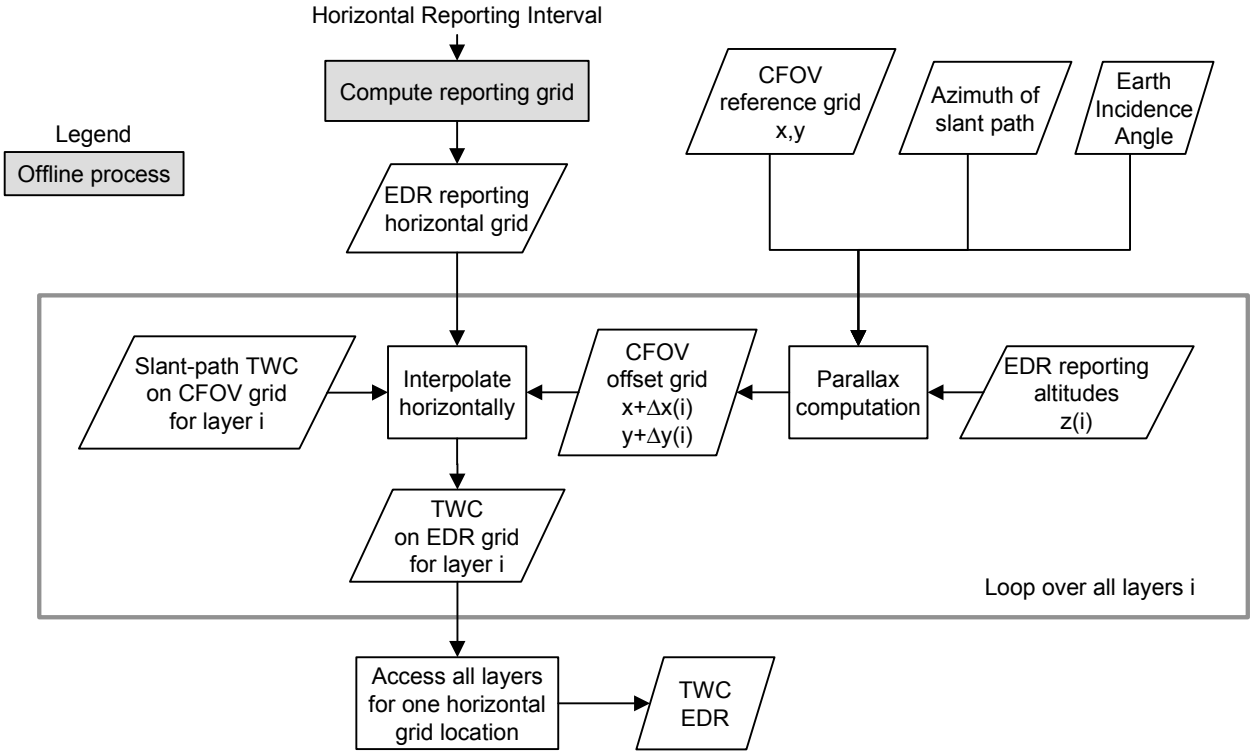

Figure 3-3: Processing flow for vertical registration for the TWC EDR algorithm.

3.3.2 Algorithm inputs

Table 3-1: TWC algorithm inputs

Data	Type	Source	Usage
20-km CFOV brightness temperatures	Dynamic, continuous	Footprint matching algorithm	Precipitating cloud algorithm
Latitude/longitude at surface	"	SDR	EDR reporting
Time/date	"	SDR	EDR reporting
Cloud cover	"	VIIRS	EDR product generation
Cloud top	“	VIIRS	EDR product generation
Water vapor profile	“	Core module	EDR product generation
Temperature profile	“	Core module	EDR product generation
Cloud liquid water	“	Core module	EDR product generation
Cloud top pressure	“	Core module	EDR product generation
Cloud top thickness	“	Core module	EDR product generation
Surface pressure	“	Core module	EDR product generation
Quality control parameters	“	Core module	EDR product generation and reporting
Liquid Water Path	“	Precipitation module	EDR product generation

3.3.3 Algorithm outputs

Table 3-2: TWC algorithm outputs

Output parameter
Total water content profile
Quality flag
Latitude/longitude at surface
Time/date

4 Algorithm Performance

4.1 Description of Test Data and Test Methods

The test data for evaluating the TWC for non-precipitating clouds consist of the data applied to the core module, described in ATBD Vol. 2. The test data for precipitating clouds are described in ATBD Vol. 5: Precipitation.

4.2 Performance in non-precipitating conditions

TWC retrieval performance is highly sensitive to surface type and, in particular, to the surface emissivity at 18/23 GHz and its uncertainty. Further discussion of surface types, their relationship to emissivity, and their frequency of occurrence are in ATBD Vol. 3: Water Vapor EDRs. Binned performance for several surface types is illustrated in Figure 4-1. The surface type has an effect for the lowest two 3-km layers of the atmosphere. Errors in the third and higher layers are very small with respect to the requirement regardless of surface type.

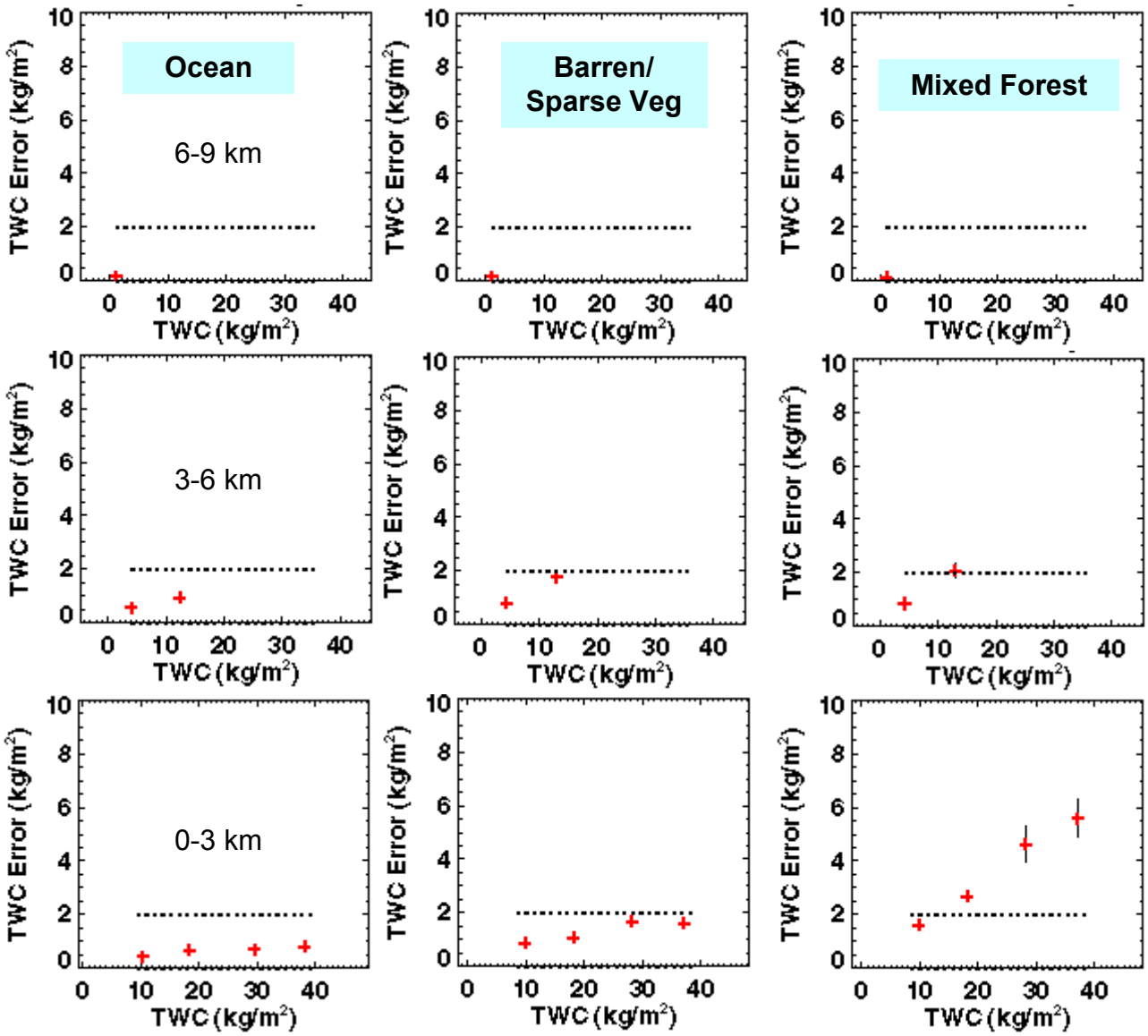

Figure 4-1: TWC measurement uncertainty as a function of true TWC (kg/m^2) for three surface types and for three 3-km layers. The test cases had a uniform distribution of cloud liquid water from 0 to 0.5 kg/m^2. The retrievals were run at 50-km CFOV size. The SRD threshold requirement is the dashed line.

Performance with respect to surface type is summarized in Table 4-1, where the errors are stratified according to 18/23 GHz emissivity for land surfaces. Errors are listed with the routine treatment of the surface emissivity constraint and for a tighter constraint that represents locations where the emissivity is stable enough that a static or dynamic emissivity database may be used. The constraint is conservatively taken to be an emissivity standard deviation of 0.04.

Table 4-1: TWC EDR performance (rms error in kg/m^2 for worst-case bin and layer) for non-precipitating clouds for various surface conditions (19 GHz H-polarization) and other measurement conditions.

	emis sd<0.04	Ocean	Land <0.86	Land 0.86-0.90	Land 0.90-0.98
Clear	N	0.56	1.40	1.99	5.25
	Y		1.15	1.72	5.09
Cloudy	N	0.79	1.68	2.25	5.59
	Y		1.46	2.09	5.46
Global Coverage:		71.0%	9.3%	3.9%	15.7%

4.3 Performance in precipitating conditions

4.3.1 Liquid and ice

Performance for retrieval of the sum of liquid and ice in precipitating clouds is in Figure 4-2 for ocean surfaces and Figure 4-3 for land.

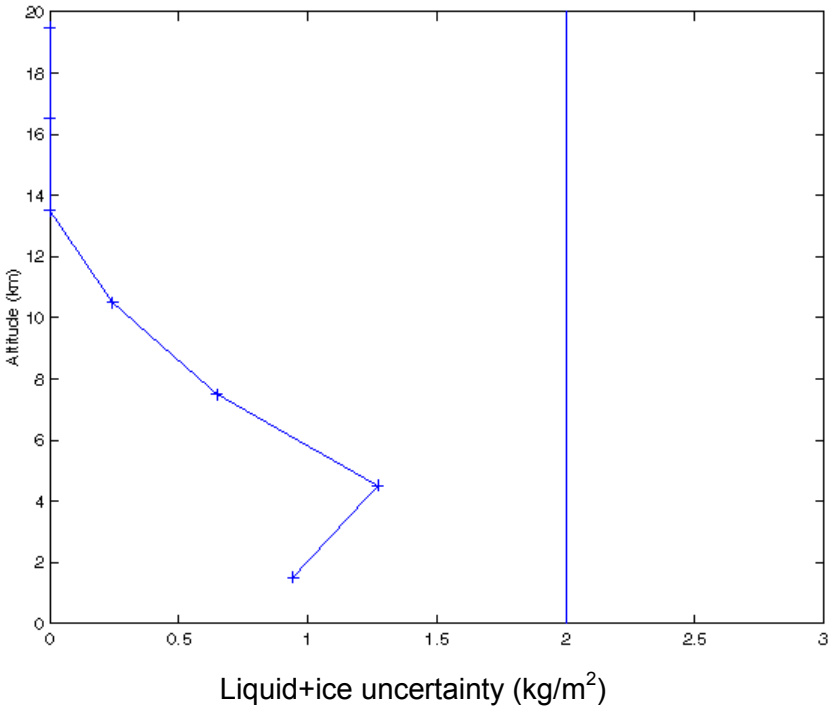

Figure 4-2: Retrieval uncertainty for the sum of liquid and ice in precipitating clouds over ocean surfaces. The threshold is marked, although it applies only after vapor uncertainty is included.

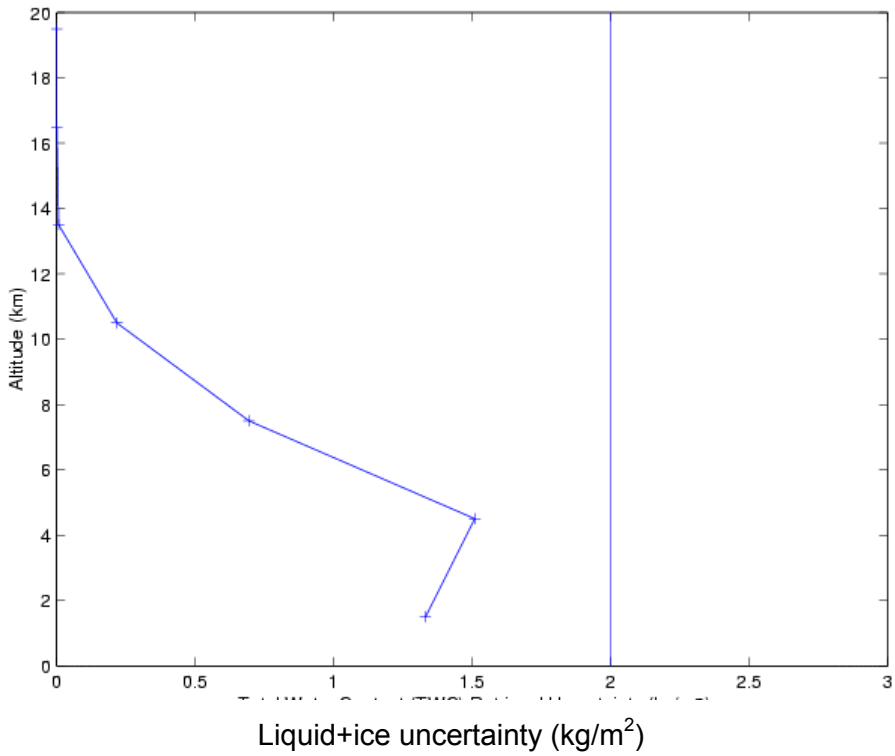

Figure 4-3: Retrieval uncertainty for the sum of liquid and ice in precipitating clouds over land surfaces. The threshold is marked, although it applies only after vapor uncertainty is included.

The performance for water vapor in precipitating conditions was analyzed with high-resolution numerical weather prediction model data. The analysis methods and its results are discussed in Appendix A of this document.

4.4 Performance summary

The nominal performance for the TWC EDR is summarized in Table 4-2. The error budgets for point measurement uncertainty and global average uncertainty are in Table 4-3 and Table 4-4, respectively. The quoted performance refers to the worst-case layer within the vertical coverage range (the performance would appear better if all data within the range were pooled before computing statistics). For point measurement, performance is computed in bins that span the applicable measurement range and the quoted performance refers to the worst-case bin unless otherwise specified.

The performance for measurement range is constrained by the scientific basis for retrieving TWC. Vapor in a 3-km layer rarely exceeds about 45 kg/m^2 in nature. Liquid and ice in a 3-km

layer does not exceed 15 kg/m^2 except in moderate-to-heavy precipitating clouds with small area coverage. To extend the range to large values of liquid and ice requires knowledge that does not yet exist about cloud structure and microphysics and their interaction with microwave radiation. Further discussion of this issue is presented in ATBD Vol. 5. The scientific basis does not exist to reliably develop and validate a TWC algorithm for a measurement range beyond 60 kg/m^2. (See also EN #46 response.)

Table 4-2: Nominal performance for the TWC EDR.

Para. No.		Thresholds	Objectives	Performance
C40.3.6-1	a. Horizontal Cell Size	20 km	10 km	20 km
C40.3.6-2	b. Horizontal Reporting Interval	20 km	10 km	20 km
C40.3.6-3	c. Vertical Cell Size	3 km	1 km	3 km
C40.3.6-4	d. Vertical Reporting Interval	Vertical cell size	Vertical cell size	Vertical cell size
C40.3.6-5	e. Horizontal Coverage	Global	Global	Global
C40.3.6-6	f. Vertical Coverage	0 - 20 km	0 - (TBD) km	0 - 20 km
C40.3.6-7	g. Measurement Range	0 - 200 kg/m² (TBR)	(TBD)	0 - 60 kg/m²
	h. Measurement Uncertainty			
C40.3.6-8	1a. Point Measurement, non-precipitating	2 kg/m^2	(TBD)	1.2 kg/m^2
	1b. Point Measurement, precipitating	2 kg/m^2	(TBD)	2.2 kg/m^2 or 15%
C40.3.6-9	2. Global Average	1 kg/m^2(TBR)	(TBD)	0.25 kg/m^2
C40.3.6-10	i. Mapping Uncertainty	7 km	7 km	3 km
C40.3.6-11	j. Swath Width	1700 km (TBR)	3000 km (TBR)	1700 km

The error budget for the TWC point measurement uncertainty is in Table 4-3. For non-precipitating cases, the error was derived by pooling stratified results from several conditions. The surface type/emissivity categories listed in Table 4-1 were combined in proportion to the global area coverage fraction, also listed in that table. Performance for the lowest 3-km layer over the most highly emissive surfaces (emissivity greater than 0.90) was excluded, and is addressed in the section covering degraded measurement conditions. Results from clear-sky retrievals were combined with results from cases where cloud liquid varied randomly from 0 to 0.5 kg/m^2. The clear-sky and cloudy results were weighted by factors of 0.68 and 0.32, respectively, to align with the observed global average cloud liquid of 0.08 kg/m^2 [0.32(0+0.5)/2=0.08]. It was assumed that a local emissivity database with emissivity standard deviation less than 0.04 could be used over half the land areas. After performing weighted

averages over these conditions for each layer and each bin across the measurement range, the worst-case bin was chosen for the error budget, in accordance with SRD requirements.

For precipitating clouds, the performance was addressed by considering a range of surface types simultaneously. The listed "default" error is for cloudy conditions and a term is included for an inflation of the water vapor retrieval error of 30% to account for errors due to interpolation and the saturation assumption. This inflation value is substantially larger than the ~10% found in the analyses discussed in Appendix A, leaving margin for the possibility of larger errors in wintertime mid-latitude environments. The percentage error for precipitating liquid and ice, based on binned performance data, is 20% of the amount of liquid plus ice or 5% of the TWC.

For the performance under non-precipitating conditions, many of the analyses on which the error budget is based were performed with direct core module retrievals because, at the time of their execution, the simulation environment was not mature enough to make it economical to perform all retrievals with the cascade feature of the core module. The net effect of the cascade depends on the global distribution of fine-scale spatial structure of water vapor, cloud, and other environmental variables, which is not known with certainty and is difficult to estimate with currently exiting datasets. The error budget term for "Default core module retrieval error" includes the effects of radiometric noise and is an estimate of the performance at 20-km cell size upon execution of the cascade. The performance values were obtained by the estimation that, averaged over the globe, the retrieval products will have errors about 5% greater than for 50-km CFOV direct retrievals. The 5% value was derived by considering the results for highly inhomogeneous scenes discussed in ATBD Vol. 1, Part 1: Integration (about 10-20% difference), and accounting for the fact that most scenes will be considerably less inhomogeneous. The water vapor inhomogeneity is the primary factor for TWC because the TWC is dominated by water vapor outside of precipitating clouds. If the net effect of the cascade is less beneficial than we have estimated, it may be necessary to produce reports for a horizontal cell size greater than 20-km in order to meet the measurement uncertainty requirements. If the net effect is more beneficial than we have estimated, the measurement uncertainties will be smaller than those we have quoted.

Following the row in Table 4-3 denoted "Net default" row are several rows (up to "Subtotal") for which the errors are additive. The numbers cited are the added retrieval errors that were found as each error source was individually simulated. Where an error budget entry is zero, that indicates

that the error term is negligible in relation to the other terms, not that the error term is identically zero.

Air mass classification was not implemented in the default retrieval simulations, so it is handled as a separate correction (error reduction of 1%) for the purposes of error budgeting.

The error budget includes two terms for spectroscopic errors. One refers to the biases between the brightness temperatures CMIS reports and brightness temperatures simulated by applying the core module radiative transfer to data representing the true environmental conditions. It is a residual in the sense that these biases are largely corrected before the water vapor retrievals are performed, using correction factors derived from calibration/validation with ground truth data (Wentz, 1997). Some differences between the CMIS measurements and the model are not sufficiently systematic to be corrected with ground truth data, and the budget includes a separate term for these errors. The error increments for ocean and land are 5% and 0.5%, respectively, of the nominal error, with a net increment of 4%.

Two sub-field-of-view effects were considered for the error budget. The budget includes a term for differences between cloud water in the direct and indirect paths. Considering the relative contribution of cloud to the TWC, the varying degree of ocean surface specularity and of cloud path differences on the 20-km scale, we estimate an error increment of 1% for non-precipitating clouds. For precipitating clouds, the water vapor component of the TWC error is dominant, while the smaller liquid/ice component is more susceptible to errors due to path differences. We estimate the net effect as a 5% error magnification for precipitating clouds. The effect of partial cloud cover, averaged over the oceans, is estimated as an error increment of 2% for non-precipitating conditions. An increment of 5% is used for precipitating conditions, accounting for the tendency of precipitating clouds to have larger spatial scales than non-precipitating clouds but for the cloud errors to be a larger part of the budget in precipitating cases.

Spatial coregistration errors involve two factors. One is the divergence of two beams that are coregistered at the surface but have different Earth incidence (zenith) angles and, hence, slightly different paths through the atmosphere. An analysis of this factor found no significant effect on vapor or liquid retrieval. The other factor is the uncertainty in the position of each channel's beam in relation to the positions of other channels. This factor was evaluated by considering several types of scene spatial structure that could cause brightness temperatures in a

misregistered channel to be different from a correctly registered channel. Effects of cloud, surface emissivity, and surface temperature structure were considered and the impact on retrieval performance was computed. Details of the analyses are in Appendix TBD of ATBD Vol. 1, Part 1: Integration. For the TWC components, coregistration errors within the requirements flowed to the sensor could cause retrieval error over ocean to increase by about 4% of the retrieval error obtained without coregistration error. The factor was about 3% over land.

The channels on CMIS are not all boresighted, so there are time offsets on the order of a few seconds between the views of the various channels. An analysis indicated that the time offsets have no significant impact on retrievals.

Uncertainty in the surface pressure, provided as external data to the core module, was found experimentally to have a very small impact on performance for layer water vapor and cloud (about 1% proportional increase in error).

Errors are introduced by the difference in spatial weighting between the horizontal cells used for validation (uniform averaging over a square) and the composite antenna pattern represented by the CFOV. Analysis of this effect is discussed in Appendix TBD of ATBD Vol. 1, Part2: Footprint Matching and Interpolation. These errors are listed as "cell mismatch error" in the budget and are about 0.15 kg/m^2 per 3-km layer for non-precipitating cases and 0.17 kg/m^2 for precipitating cases.

Table 4-3: Error (kg/m^2) budget for TWC EDR point measurement uncertainty

Term	Non-precipitating	Precipitating
Default core module retrieval error	0.96	1.20 or 10%
Interpolation into precipitating areas	N/A	0.36 or 3%
Precipitating cloud liquid and ice	N/A	1.30 or 5%
Net default	0.96	1.81 or 12%
Adjustment for cascade from 50 to 20-km HCS	0.05	0.05 or 0.5%
Adjustment for air mass classification	–0.01	–0.01 or 0.1%
Residual calibration/model bias	0.04	0.05 or 0.5%

Residual unsystematic spectroscopic error	0.04	0.05 or 0.5%
Direct/indirect-path differences	0.01	0.06 or 0.5%
Partial cloud cover	0.02	0.09 or 0.6%
Channel spatial coregistration error	0.04	0.05 or 0.4%
Channel temporal offset	0.00	0.00
Surface pressure error	0.01	0.01 or 0.1%
Subtotal	1.16	2.16 or 15%
Cell mismatch	0.15	0.17 or 1.3%
Net	1.17	2.17 or 15%

The error budget for the global average depends on the measurement biases. No surface types were excluded in this budget. The conditions excluded from reliable point measurement encompass areas of precipitation greater than 50 mm/h, which aligns with locations where the TWC in any layer is greater than the 60-kg/m^2 upper end of the measurement range. Among those excluded regions, we estimate an average moistest-layer TWC of 70 kg/m^2, considering that the frequency of occurrence of a given amount of TWC drops off quickly as a function of TWC. This average TWC would give an average retrieval error of 10 kg/m^2 if our algorithm saturates at 60 kg/m^2. The errors for the three environments listed are averaged in the budget with weighting by the percent of earth coverage of each environment. Residual calibration/model bias enters into the budget also. The other terms in the point measurement error budget are random and do not factor into the global average.

Table 4-4: Error (kg/m^2) budget for TWC EDR global average measurement uncertainty

Term	Environment	% coverage	Error
Algorithm bias	Non-precipitating	90	0.14
	Precipitating < 50 mm/h	9.5	0.27
	Precipitating > 50 mm/h	0.5	10.00
	Net		0.20
Residual calibration/model bias			0.01
Margin			0.04
Overall Net			0.25

4.5 Summary of performance under degraded measurement conditions

Performance under degraded measuring conditions is lised in Table 4-5 and the excluded condition is indicated in Table 4-6.

Table 4-5: Summary of TWC performance under degraded measurement conditions.

Condition	Indicator	Measurement uncertainty for point measurement
Lowest 3-km layer over moderate and dense vegetation	18 GHz H emissivity > 0.9	6.5 kg/m^2 or 30%
VIIRS cloud cover not available and non-precipitating		1.4 kg/m^2
VIIRS cloud cover or cloud top not available, and moderate or heavy ice cloud present	Ice water path ≥ 0.03 kg/m^2 or ice particle D_{me} ≥ 300 □m	Greater of 2.2 kg/m^2or 15%
Prior-pass CrlS water vapor or VIIRS land surface temperature not available; 0 to 3 km height range, non-precipitating		1.3 kg/m^2

Table 4-6: TWC excluded condition.

Condition	Exclusion
Precipitation rate greater than 50 mm/h	Measurement uncertainty, point measurement

4.6 Special considerations for Cal/Val

4.6.1 Measurement hardware

4.6.2 Field measurements or sensors

4.6.3 Sources of truth data

5 Practical Considerations

5.1 Numerical Computation Considerations

5.2 Programming/Procedure Considerations

5.3 Computer hardware or software requirements

5.4 Quality Control and Diagnostics

5.5 Exception and Error Handling

5.6 Special database considerations

5.7 Special operator training requirements

5.8 Archival requirement

REFERENCES

Alishouse, J. C., J. B. Snider, E. R. Westwater, C. T. Swift, C. S. Ruf, S. A. Snyder, J. Vongsathorn, and R. R. Ferraro, 1990: Determination of cloud liquid water content using the SSM/I. *IEEE Trans. Geosci. Remote Sensing*, **28**, 817-821.

Bohren, C. F., and D. R. Huffman, 1983: *Absorption and Scattering of Light by Small Particles*. Wiley, New York.

Chang, A. T., and T. T. Wilheit, Remote sensing of atmospheric water vapor, liquid water, and wind speed at the ocean surface by passive microwave techniques from the Nimbus 5 satellite. *Radio Sci*., **14**, 793-802.

Gasiewski, A. J., 1992: Numerical sensitivity analysis of passive EHF and SMMW channels to tropospheric water vapor, clouds, and precipitation. *IEEE Trans. Geosci. Remote Sensing*, **30**, 859-870. Errata: 1993, **31**, 306.

Greenwald, T. J., G. L. Stephens, T. H. Vonder Haar, and D. L. Jackson, 1993: A physical retrieval of cloud liquid water over the global oceans using Special Sensor Microwave/Imager (SSM/I) observations. *J. Geophys. Res*., **98**, 1847-1848.

Greenwald, T. J., C. L. Combs, A. S. Jones, D. L. Randel, and T. H. Vonder Haar, 1997: Further developments in estimating cloud liquid water over land using microwave and infrared satellite measurements. *J. Appl. Meteor*.,**36**, 389-405.

Greenwald, T. J., C. L. Combs, A. S. Jones, D. L. Randel, and T. H. Vonder Haar, 1999: Error estimates of spaceborne passive microwave retrievals of cloud liquid water over land. *IEEE Trans. Geosci. Remote Sensing*, **37**, 796-804.

Jones, A. S., and T. H. Vonder Haar, 1990: Passive microwave remote sensing of cloud liquid water over land regions. *J. Geophys. Res*., **95**, 1667-1668.

Lipton, A. E., M. K. Griffin, and A. G. Ling, 1999: Microwave transfer model differences in remote sensing of cloud liquid water at low temperatures. . *IEEE Trans. Geosci. Remote Sensing*, **37**, 620-623.

Liu, G., and J. A. Curry, 1993: Determination of characteristic features of cloud liquid water from satellite microwave measurements. *J. Geophys. Res*., **98**, 5069-5092.

Phalippou, L., 1996: Variational retrieval of humidity profile, wind speed and cloud liquid-water path with the SSM/I: Potential for numerical weather prediction. *Quart. J. Roy. Meteor. Soc*., **122**, 327-355.

Weng, F., and N. C. Grody, 1994: Retrieval of cloud liquid water using the special sensor microwave imager (SSM/I). *J. Geophys. Res*., **99**, 2553-2555.

Wentz, F. J., A well calibrated ocean algorithm for SSM/I, *JGR*, **Vol 102**, pp 8703-8718, 1997.

LIST OF ACRONYMS

AER	Atmospheric and Environment Research
ATBD	Algorithm Theoretical Basis Document
CFOV	Composite Field of View
CLW	Cloud Liquid Water
CMIS	Conical-Scanning Microwave Imager/Sounder
EDR	Environmental Data Record
FOV	Field Of View
IPO	Integrated Program Office
LWP	Liquid Water Path
NPOESS	National Polar-orbiting Operational Environmental satellite System
QC	Quality Control
SDR	Sensor Data Record
SRD	Sensor Requirement Document
SSM/I	Special Sensor Mirowave/Imager
SSM/T-2	Special Sensor Mirowave/Temperature-2
TBD	To Be Determined (by contractor)
TDR	Temperature Data Record
TWC	Total Water Content
VIIRS	Visible/Infrared Imager/Radiometer Suite

APPENDIX A: TWC Errors Due to Interpolation of Water Vapor in Precipitating Areas

Ross N Hoffman and Alan Lipton

A.1 Introduction

In this study we quantify the effect of interpolation in rainy cases on the estimated 3-km thick TWC layer amounts. The high resolution model simulation used is from the University of Wisconsin case study (denoted Friuli) of an extreme precipitation event on a 2.34 km grid. These data are described in ATBD Vol. 1, Part 1, Appendix A.

For this study, the high resolution model data are averaged in 8x8 grid cell blocks to an effective resolution of ~20 km. These 20 km data are considered truth here. The estimated three-dimensional fields are generated by eliminating all air temperature (T_a) and water vapor mixing ratio (r(v)) data where it is precipitating. The remaining data are spatially interpolated to fill in the holes where it is raining using the Gaussian filter approximation to the recursive filter described in ATBD Vol. 1, Part 2, with some modification described below (A.2). The interpolated r(v) is used to estimate the true r(v) above cloud top and the interpolated T_a and an assumed constant relative humidity (RH) of 0.85 are used to estimate the true r(v) below cloud top. The true and estimated r(v) are then converted to the 3-km thick TWC layer amounts and compared using the statistics described in ATBD Vol. 1, Part 1, Appendix A. Examples are shown in section 3 of this appendix and the resulting statistics are given in section 4. In brief, the resulting rms relative errors (RE) are modest, varying from 10 to 20% increasing with height. For comparison a second estimate of r(v) is generated using the true T_a and the assumed constant 0.85 RH. The rms RE in this comparison are ~10%.

A.2 Methodology

The following steps were followed.

1. The high resolution model fields were averaged over 8×8 horizontal blocks of grid points. This reduces the resolution from 2.34 km to 18.72 km. If any one of the grid points in a block is

missing, the averaged value is set to missing. Missing values occur below the height of the model topography. The result is taken to be the truth in this study.

2. The rainy locations in the true fields of T_a and r(v) are masked (i.e. set to missing). A rainy location is indicated whenever the rainrate (RR) exceeds 0.1 mm/hr. In the Friuli case, for the four times available, this masks ~40% of the domain. Other variables—air density ρ_a, ice mixing ratio r(i), and liquid mixing ratio r(l)—are not masked. Thus the true values of these variables are used where needed in what follows.

3. The T_a and r(v) fields are interpolated to fill in the missing values. This actually fills in missing values under topography as well, but these are ignored once the interpolation is complete. The interpolation is strictly horizontal and univariate, and uses the five step Gaussian filter described in ATBD Vol.1, Part 2, with two modifications: 1) the original field values are not allowed to change, and 2) the first step of the filter, the one with the largest scale parameter, is repeated until all missing values are filled in. This use of the largest scale parameter is needed because the rainy areas are large in size.

4. Below cloud top the interpolated r(v) is not used. Instead the interpolated T_a, and an estimated RH of 0.85 are used to estimate r(v), according to

$$r(v) = RH\ r_{sat}(T_a)$$

The RH value of 0.85 was derived by examining one time for the Friuli case, as described in A.3 below. Calculation of the saturated r(v) and any required conversion use the standard textbook formulae (Dutton, 1976, Chapter 8). Cloud top is defined by integrating water ice and liquid from the top of the atmosphere downwards until a critical value is exceeded. In other words, cloud top height, z_{ct} is the maximum z for which

$$H(z) = \int_z^\infty r(i) + r(l)\ \rho_a\ dz > 0.10\ kg/m^2$$

Here H(z) is the overburden of hydrometeors and cloud particles. For error budgeting, a second estimate of r(v) is generated using the true T_a and the assumed constant 0.85 RH.

5. True and estimated r(v) multiplied by air density ρ_a (kg/m^3) is integrated for three layers in the troposphere (low, mid, high) to obtain integrated water vapor (IWV) according to:

Variable	IWV(low)	IWV(mid)	IWV(high)
Bottom (km)	1	3	6
Top (km)	4	6	9

The use of a 1-km base for the first layer is for computational convenience, considering that the model data are provided on a fixed-altitude grid where some points below 1 km intersect the terrain.

6. For any field z, denoting the true field by z_s and the estimated field by z_g, in analogy with definitions of A.4, we define the absolute error (AE) of z as

$$z_{ae} = z_s - z_g$$

and the relative error (RE) of z as

$$z_{re} = (z_s - z_g)/\max(z_s, z_g)$$

A.3 Examples

Figure A.1 shows the true RH cross section along the line y=120 km in the innermost model domain averaged to ~20 km resolution. The scale for RH is indicated below the main plot. Horizontal lines indicate the three key height levels of 3000, 6000 and 9000 m. The averaged model topography is indicated by the lower heavy red line. Vertical bars below topography indicate rainy points. The dark heavy contour indicates the cloud top determined by H(z) = 0.10 kg/m^2. Light contours are for other values of H(z), obtained by repeated halving and doubling of the critical value of 0.10 kg/m^2. Note the very dry area aloft between 3000 and 6000 m at the left of the plot. Also note that grid points 2 and 3 are rainy and that this dry layer is below cloud top. The corresponding T_a cross section is shown in Figure A.2. In this figure we indicate which points will have to be estimated from interpolated T_a and a constant RH value.

To determine the constant RH value we took all rainy locations below cloud top and examined the RH statistics for this sample. The result is shown in Figure A.3. The value of 0.85 plus or

minus 0.16 for these “saturated” points should be contrasted with 0.43 plus or minus 0.35 for all other points for this case at this time. In what follows we use 0.85 as the constant estimate of RH for rainy points below cloud top.

Figure A.4 shows the true field of IWV(mid). The green lines and numbers indicate latitude and longitude. The dark heavy line is the coast line. For reference Venice is located at 45:27N, 12:21E, near the center of the plot. The dashed line indicates the location of the cross sections described before. Figure A.5 shows the estimated IWV(mid) for this case and Figure A.6 and Figure A.7 show the AE and RE respectively. It is clear in the error plots which regions of the domain have been filled in. Note the red area on the left edge of the error plots which corresponds to the dry area noted in the cross section of the true fields.

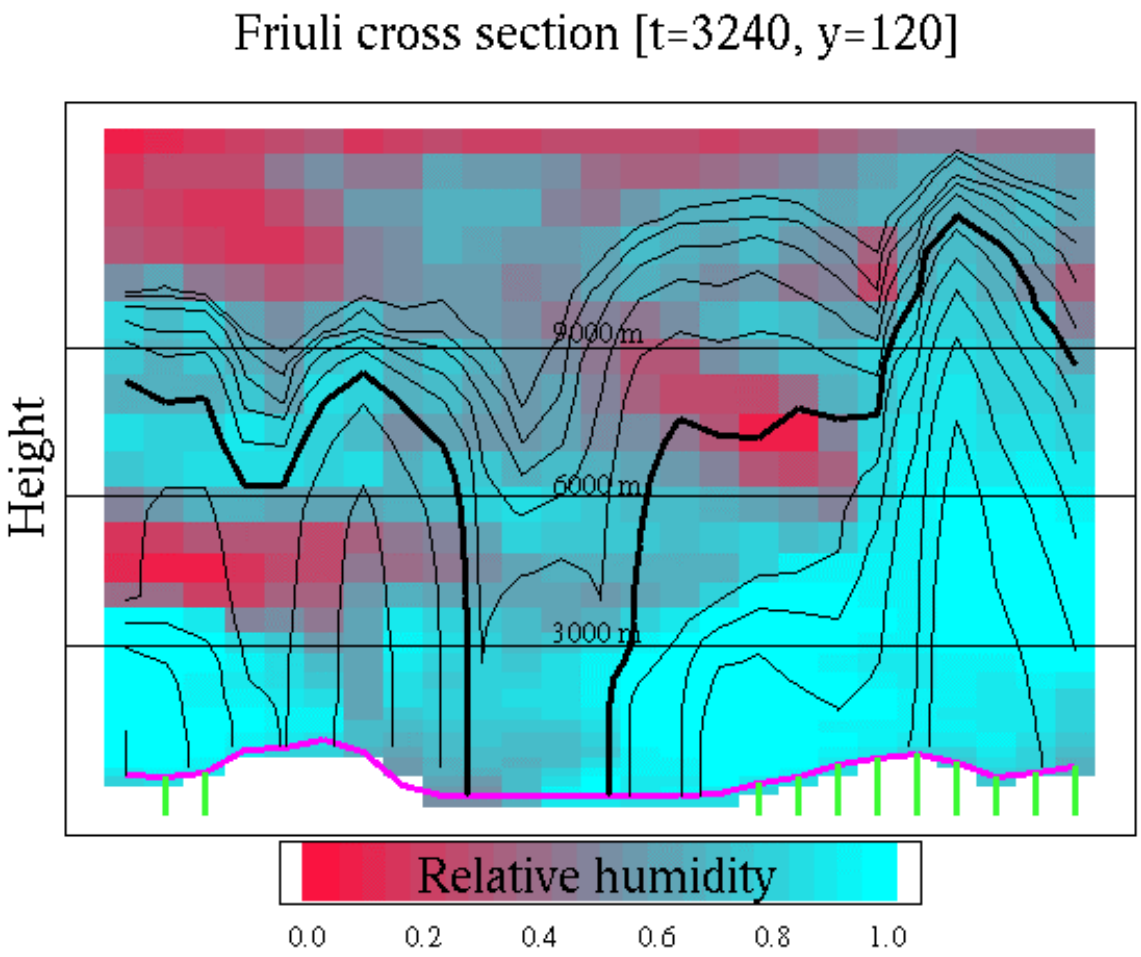

Figure A.1 Vertical cross section of RH for the Friuli case at forecast hour 54, and at y coordinate 120 km. The scale for RH is indicated below the main plot. Horizontal lines indicate the three key height levels of 3000, 6000 and 9000 m. The averaged model topography is indicated by the lower heavy red line. Green vertical bars below topography indicate rainy points. The dark heavy contour indicates the cloud top determined by $H(z) = 0.10$ kg/m^2. Light contours are for other values of H(z), obtained by repeated halving and doubling of the critical value of 0.10 kg/m^2.

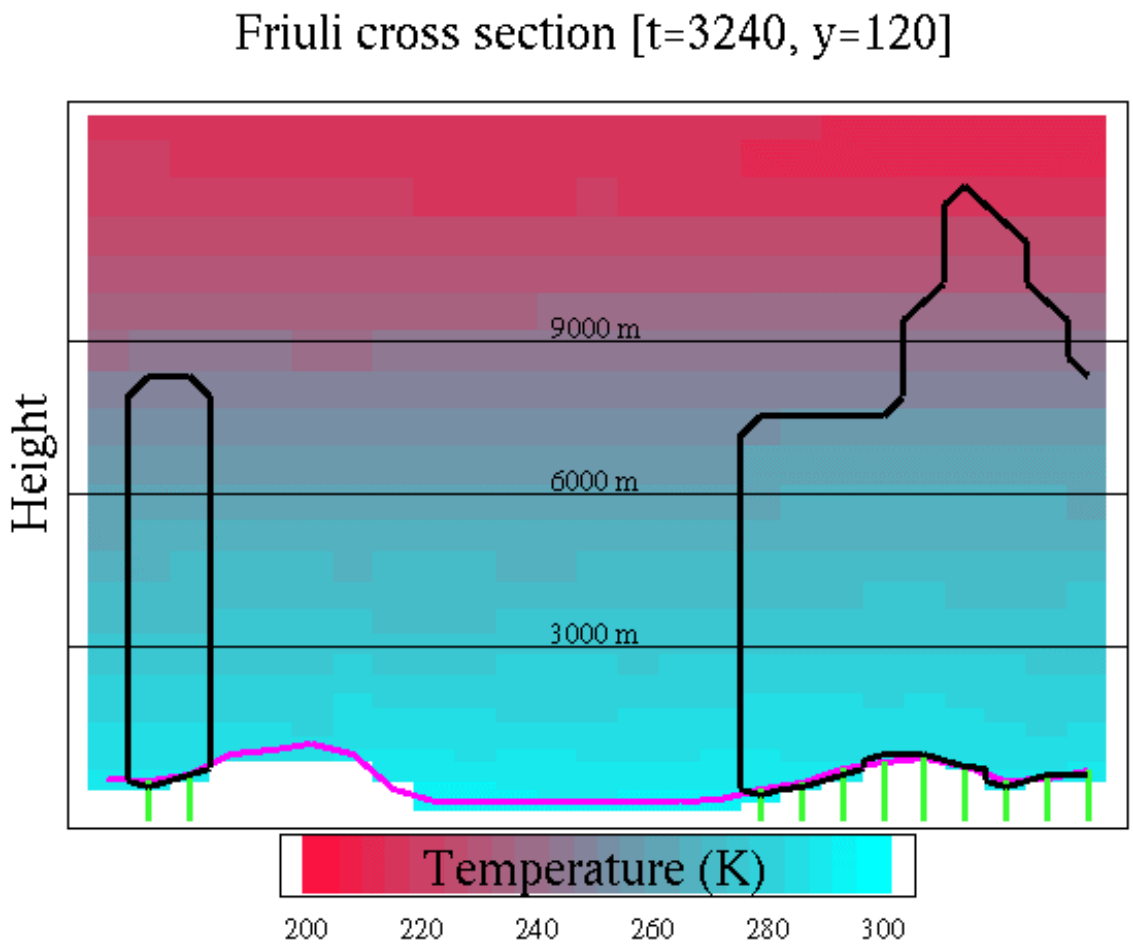

Figure A.2 Vertical cross section of T_a, as in Figure A.1. Here the region within the dark heavy contour indicates those points which will estimated using a constant RH value.

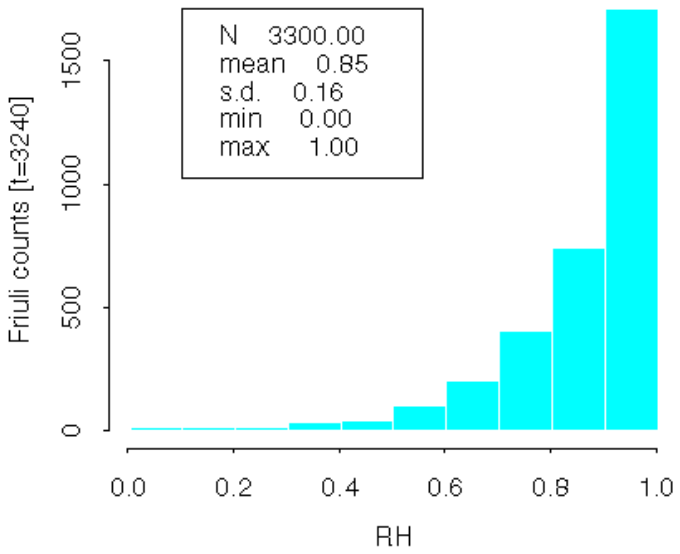

Figure A.3 Histogram of RH for the Fiuli case at forecast hour 54, for rainy points below cloud top.

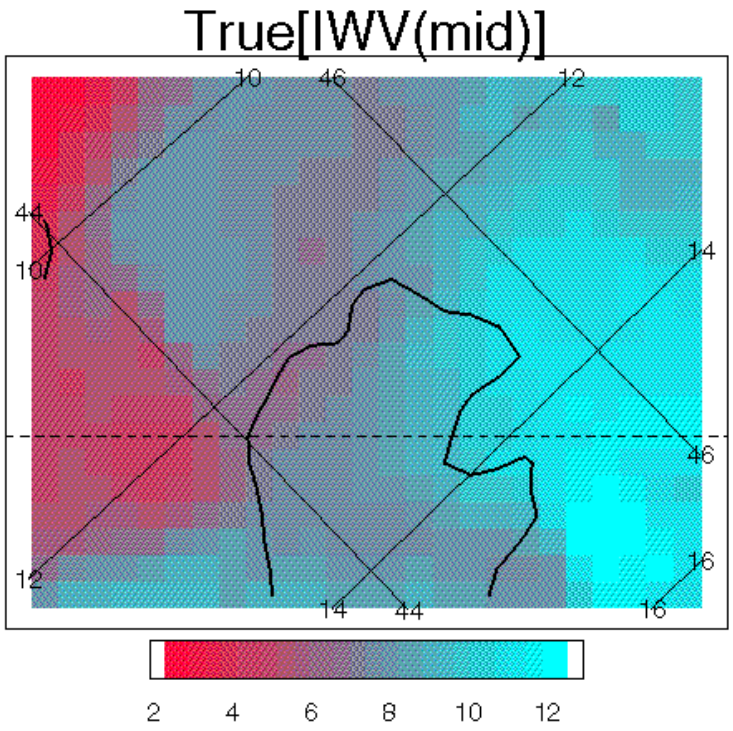

Figure A.4 The true IWV(mid) field (kg/m^2) for the Fiuli case at forecast hour 54. [The dashed line marks y=120 km, i.e. the cross section shown in Figure A.1.]

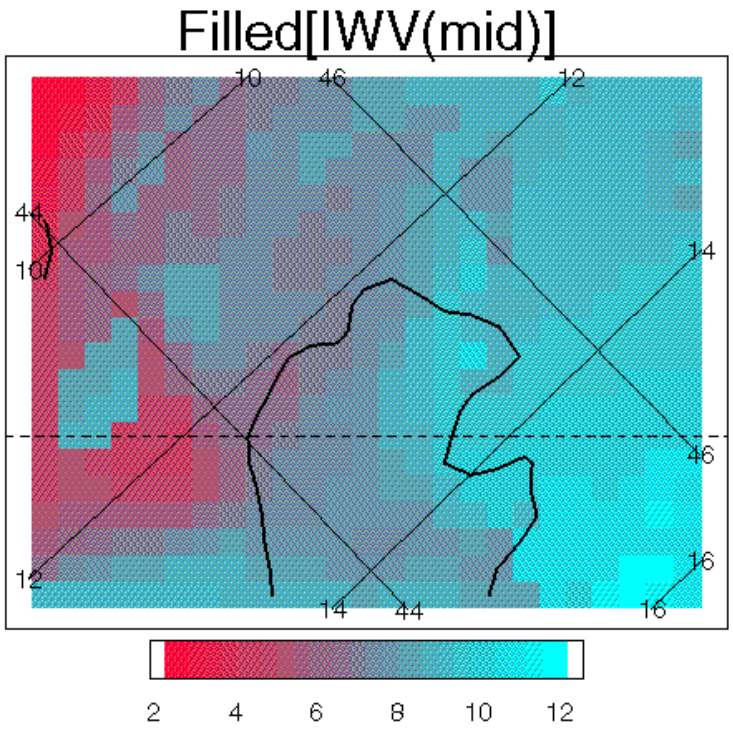

Figure A.5 The estimated IWV(mid) field (kg/m^2) for the Fiuli case at forecast hour 54.

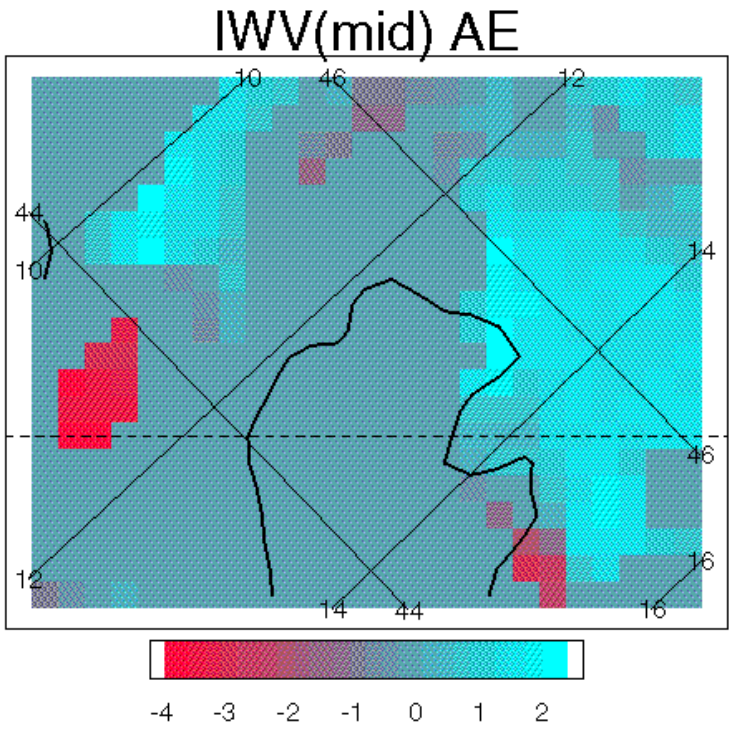

Figure A.6 The IWV(mid) field (kg/m^2) AE for the Fiuli case at forecast hour 54.

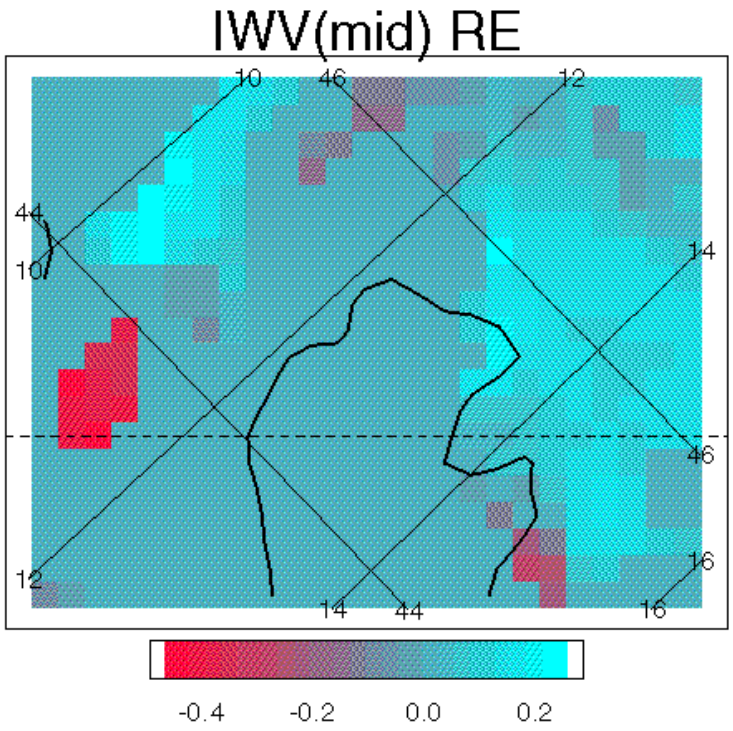

Figure A.7 The IWV(mid) field (kg/m^2) RE for the Fiuli case at forecast hour 54.

A.4 Statistics

Results are given for IWV in three layers, 1-4, 3-6, and 6-9 km, denoted IWV(low), IWV(mid), and IWV(high).

RMS statistics calculated over all four Friuli times, but for the rainy areas only are:

	true [kg/m^2]	AE(I) [kg/m^2]	RE(I) [%]	AE(T) [kg/m^2]	RE(T) [%]
IWV(low)	20.30	2.220	10.26	2.060	9.68
IWV(mid)	10.20	1.320	12.71	1.130	10.89
IWV(high)	2.31	0.350	18.44	0.312	12.51

Here, I indicates interpolated T_a and $r_{sat}(T_a)$ are used to estimate r(v) and T indicates the true values are used. Note that these are small samples, typically 200 points per time for the upper levels, and 150 points per time for IWV(low).

A.5 Discussion

Error due to interpolating across rainy areas to estimate the integrated water (IWV) in 3 km thick layers are found to be fairly small even in the very extreme situation studied. We find rms relative errors (RE) vary from 10 to 20% increasing with height. A large part of this error is due to the assumption of a constant 0.85 RH in the rainy subcloud region. Better estimates of the RH profile would reduce this part of the error. Also a very simple multi-pass Gaussian filter was used as the interpolation procedure. Reduced interpolation errors as a result of using better interpolation procedures should reduce this part of the IWV error. Interpolation in the present case is difficult because of the large size of the rainy areas, and the presence of rainy areas at the edge of the domain. We showed the method does poorly when dry air is present below cloud top. In some cases we anticipate that cirrus anvils will obscure very dry air below the cirrus level, but above low precipitating clouds.

Reference:

Dutton, J. A., 1976: "The Ceaseless Wind", McGraw-Hill, New York, pp. 579.